AIAA JOURNAL
Vol. 34, No. 11, November 1996

Novel Approach to Aerodynamic Analysis Using Analytical/Numerical Matching

Donald B. Bliss* and Ronald J. Epstein†
Duke University, Durham, North Carolina 27708-0300

Analytical/numerical matching (ANM) is a hybrid scheme combining a low-resolution global numerical solution with a high-resolution local solution to form a composite solution. ANM is applied to lifting surfaces in steady potential flow to calculate the aerodynamic loading and associated circulation distribution. The solution methodology utilizes overlapping smoothed doublets and local corrections to calculate the doublet strength distribution along the airfoil chord. The global low-resolution solution is calculated numerically using smoothed doublet solutions to the linear potential equation, and converges quickly. Simultaneous local corrections are done with high-resolution local analytical solutions. The global numerical solution is asymptotically matched to the local analytical solutions via a matching solution. The matching solution cancels the global solution in the near field, and cancels the local solution in the far field. The method is very robust, offering insensitivity to control-point location. No explicit wake geometry is assumed; therefore, a fixed- or free-wake model can be used. ANM provides high-resolution calculations from low resolution numerics with analytical corrections, while avoiding the subtlety involving singular integral equations, and their numerical implementation. The approach provides a novel alternative treatment to lifting-surface aerodynamics.

Introduction

PANEL methods,[1] or singularity methods, are a cornerstone of modern aerodynamic analysis. These methods construct aerodynamic flowfields from the superposition of simpler building-block solutions of the governing equations distributed over the body surfaces. The appropriate strengths of these elementary solutions are determined by the application of surface boundary conditions. Panel methods are used to analyze compressible, steady and unsteady, potential flow over wings and bodies for a variety of applications including performance, loads analysis, aeroelasticity, vibration, interactional and interference effects, and acoustics.

Although these methods have been in use for a number of years, and have been the subject of much research and refinement, they can possess significant shortcomings. Zero-thickness lifting-surface methods can be sensitive to the location of the control points at which the boundary conditions are applied. Certain rules, such as the well-known $\frac{1}{4}$–$\frac{3}{4}$ chord rule for vortex lattice, must be strictly adhered to or incorrect answers will result.[2] Panels must be of regular shape and arrangement, partly because of this sensitivity. Problems may arise when panel sizes or orientations vary rapidly, when panels also must be compatible with a separate grid for structural analysis, and when other surfaces or wakes are in close proximity. The analysis of free wakes by these methods poses a particular problem because wake motion leads to irregular distortion of the constituent panels, and their proximity and orientation relative to other panels on aerodynamics surfaces is difficult to anticipate. Some of these problems have been addressed with higher-order panel techniques[3,4] only in the context of steady aerodynamics, however.

Finally, there are other difficulties and subtleties associated with the numerical implementation of zero-thickness lifting-surface methods. These methods are the numerical embodiment of a singular integral equation having a kernel function whose discretization is open to interpretation, leading to possible ambiguity in the meaning of computed results. For an extensive review of panel methods, the reader may wish to consult the review papers of Erickson,[1] Johnson,[5] Margason,[6] and Landahl and Stark.[7]

Received May 17, 1995; revision received May 23, 1996; accepted for publication May 30, 1996; also published in *AIAA Journal on Disc*, Volume 1, Number 4. Copyright © 1996 by the American Institute of Aeronautics and Astronautics, Inc. All rights reserved.

*Associate Professor, Department of Mechanical Engineering and Materials Science. Member AIAA.

†NASA GSRP Fellow, Department of Mechanical Engineering and Materials Science. Member AIAA.

Given the many years of research focused on singularity methods, it should be stressed that the present research involves a novel and innovative reformulation of the fundamental approach to singularity methods, with the goal of alleviating some of the shortcomings and difficulties associated with them. The basis for this reformulation is a new analysis technique called analytical/numerical matching (ANM). The method is applied to lifting surfaces in both two- and three-dimensional steady potential flow to calculate the aerodynamic loading.

ANM

ANM is a hybrid technique that combines analytical and numerical solutions by a matching procedure. ANM allows a global low-resolution numerical solution and a local high-resolution analytical solution to be combined formally by asymptotic matching to construct an accurate composite solution. Both the numerical and the analytical solutions are simpler and more easily obtained than the solution of the original problem, and the overall solution procedure is accurate and computationally efficient. The ANM approach provides a high degree of spatial resolution in local areas without great computational burden.

ANM is a general analysis method originally developed by D. B. Bliss for application to problems in vortex dynamics and rotorcraft free-wake analysis.[8–11] Recently, ANM has been applied to problems involving acoustic radiation and structural–acoustic scattering from fluid-loaded structures with discontinuities. In all of these cases, accurate solutions were obtained with significant reductions in computational cost. The present work involves further development of ANM and its application to wing aerodynamics.

In ANM, an artificial smoothing of the physical problem is introduced. The smoothing length scale must be smaller than the large length scales in the problem, but larger than the scale of numerical discretization. Because the smoothing length scale is larger than the scale associated with the numerical discretization, the numerical solution of the smoothed problem is very accurate. However, the actual problem has a physical length scale smaller than the numerical discretization. The local region associated with the small scale is solved separately (usually analytically, but sometimes numerically) as a high-resolution local problem that captures the small scales and rapid variations. This local problem, because of its idealizations, is valid only in the local region.

The numerical problem and the local problem are combined by asymptotic matching to form a composite solution. ANM utilizes a matching procedure similar to the method of matched asymptotic

expansions (MAE), but otherwise the methods are different. The ANM approach requires a matching solution that is similar to the local problem, but is solved with the smoothing imposed. The smoothing length scale is the largest scale associated with the local region, but still small compared to global scales. This scale separation allows these local solutions (high-resolution and matching) to be solved with simplified geometry. The composite solution then is given by the low-resolution global numerical solution plus the high-resolution local solution minus the matching solution, namely:

Composite Soln. = Low Resolution Numerical Soln.

+ High-Resolution Local Soln.

− Smoothed Local Matching Soln.

In the local region, the matching solution subtracts the local error associated with the smoothed numerical solution, leaving the local solution. Far from the local region, the local solution and the matching solution cancel, because they become identical beyond the smoothed region. For the method to work well, the smoothing must be chosen to achieve a mathematical overlap so that the transition zone between the local and the numerical solutions is accurate.

The application of ANM to aerodynamics proceeds as follows: The ANM smoothed global solution is constructed by an overlapping distribution of smoothed aerodynamic doublets, shown in Fig. 1. A smoothed doublet is analogous to the familiar singular doublet, except that there is a smooth spatial distribution of doublet strength and they are everywhere nonsingular.

Next, as shown in Fig. 1, the ANM local solution for aerodynamics is constructed from the difference between a high-resolution local solution based on singular doublets, and a corresponding smoothed local solution, called the matching solution, based on smoothed doublets. The difference between these solutions cancels far away, because they have the same far-field behavior. Therefore, the far-field shape and behavior are unimportant, allowing very simple solution forms to be used. Appropriate high-resolution local solutions on surfaces and near edges can be found by separation of variables, or by integrals over singular doublet distributions of infinite or semi-infinite extent. Matching solutions can found by integration over corresponding smoothed doublet distributions, or by a special variable separation technique combined with an equivalent singularity displacement method called the split-sheet analogy.

The ANM composite solution is formed from the low-resolution global solution, plus the high-resolution local solution, minus the low-resolution local matching solution. At a point of evaluation on the surface, the global solution provides the correct far field, but its near-field contribution is smoothed. Subtracting the matching solution removes the local smoothing effect of the global solution,

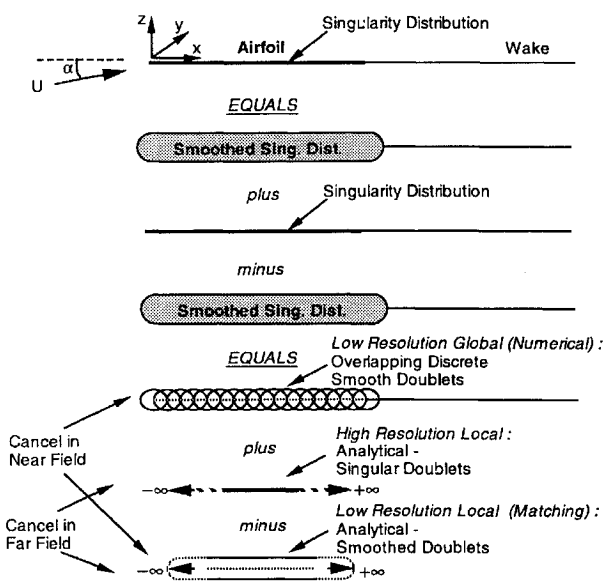

Fig. 1 Schematic representation of the ANM solution methodology for aerodynamics.

and adding the high-resolution local solution provides the local fine structure. The high-resolution local solution and the matching solution cancel in the far field, leaving the global contribution. When done properly, the final answer is independent of the degree of smoothing over a wide range of smoothing length-scale values. This independence demonstrates that a region of solution overlap has been achieved.

Problem Formulation

Governing Equations

Panel methods use a surface singularity distribution to solve the linear potential flow equation for an arbitrary geometry. The use of the velocity potential for inviscid, irrotational flow reduces the problem to the solution of an integral equation for a scalar function on a two-dimensional surface. For the case of subsonic incompressible flow, the governing equation is linear without further approximation.

The governing equation for incompressible flow is Laplace's equation[12] and can be written in rectangular coordinates as

$$\frac{\partial^2\varphi}{\partial x^2}+\frac{\partial^2\varphi}{\partial y^2}+\frac{\partial^2\varphi}{\partial z^2}=0 \tag{1}$$

In general, Eq. (1) can be transformed in the Prandtl–Glauert equation,[12] which governs linearized, compressible, steady potential flow through the Göthert transformation.[12] The difficulty, however, is that the Neumann boundary condition in the transformed space does not correspond to the normal component of the velocity in the physical space.

Using the appropriate form of Green's theorem,[13] the solution to Eq. (1), in integral form, can be found as[12,14,15]

vspace*-2pt

$$\varphi(p)=-\frac{1}{4\pi}\iint_{S_b+S_w}\left[\sigma_\omega\frac{1}{r}-\mu_\omega\frac{\partial}{\partial n}\left(\frac{1}{r}\right)\right]\mathrm{d}S \tag{2}$$

where $r=|\boldsymbol{X}_p-\boldsymbol{X}|$. Equation (2) gives $\varphi(p)$ in terms of a distribution of simple sources and doublets along the boundary S_b+S_w, where b denotes body, w denotes wake, p is the point of evaluation, and σ_ω and μ_ω are the source and doublet strengths, respectively. The doublet orientation is specified positive aligned with the z axis, such that in the double source limit is taken with the source above the sink. Most recent methods are based on some form of this equation.[6]

The Neumann boundary condition is satisfied at the surface, where the specified normal velocity v_n must be equal to the velocity induced by the integrated surface distribution of monopoles and doublets, found by taking the derivative of Eq. (2) normal to the surface S_b. The monopole source term is not always required, and valid solutions can be composed with only doublet distributions.[16] In fact, this is the case for the aerodynamic lifting problem without thickness, where a continuous normal velocity across the boundary is desired. Taking the normal derivative of Eq. (2), it then can be written without the monopole source term as

$$v_n(p)=\boldsymbol{n}\cdot\left(\frac{1}{4\pi}\iint_{S_b+S_w}\left\{\mu_\omega\nabla\left[\frac{\partial}{\partial n}\left(\frac{1}{r}\right)\right]\right\}\mathrm{d}S\right) \tag{3}$$

for p on S_b+S_w. Equation (3) is a homogeneous Fredholm integral equation of the first kind, relating the unknown doublet strength distribution on S_b to the specified normal velocity on S_b. The doublet strength distribution in the wake can be explicitly determined from the doublet strength distribution along the body surface S_b. Typically, following the Kutta condition, the wake strength is convected from the trailing edge, thereby ensuring finite velocities at the trailing edge. The wake is a material surface in the fluid and cannot support a finite pressure jump. Therefore, the doublet strength in the wake must be set such that there is no pressure jump across the wake surface.

In general, a numerical method is created when the surface is discretely approximated by a contiguous set of small elements or panels. Computational panels are formed by integrating the singularity distribution with a parameterized strength dependence over a small subdomain. Typically, the panels are quadrilaterals, and on each element, a collocation point is identified. In most cases, the collocation point must be at a specific location on the computational

element. The singularity strength can be constant over the panel or vary in some higher-order fashion. In general, the higher-order methods are more robust.[3,4] Collocation point positioning can be critical for lower-order methods, where the proper positioning is needed to correctly model the Kutta condition at the trailing edge. In practice, the Kutta condition is implemented by attaching the wake to the trailing edge, evaluating the wake strength from μ_{te}, the doublet strength at the trailing edge panel, and convecting μ_{te} in the wake with the local freestream velocity. The integral equation and the boundary conditions are evaluated at the collocation points, thus giving rise to a set of algebraic equations for the unknown singularity strength μ, based on the discrete approximation of Eq. (3):

$$\left(\frac{\partial \varphi}{\partial n}\right)_k = \frac{1}{4\pi} \sum_{\substack{\text{body} \\ \text{and wake}}} A_{kj}\mu_j \tag{4}$$

The influence coefficients A_{kj} only depend on the body and wake geometry and therefore are fixed for rigid body motion and a prescribed wake geometry.

The theory behind the numerical implementation of the Kutta condition, although incomplete, is more complex and subtle than practice would suggest.[17] In their 1969 paper on the doublet lattice method, Albano and Rodden[18] said, "Furthermore, the Kutta condition has not been imposed. However, from numerical experimentation with this technique, it has become apparent that the Kutta condition will be satisfied when each downwash point is at the $\frac{3}{4}$ chord point at midspan of a box." To date, all zero-thickness lifting-surface methods, such as vortex lattice methods, must invoke some sort of $\frac{1}{4}$–$\frac{3}{4}$ chord placement rule per panel to satisfy the Kutta condition. The solution to the aerodynamic problem is not unique; there are any number of different solutions, each corresponding to the amount of circulation specified. The Kutta condition is satisfied by assigning the proper amount of circulation needed for the flow to leave from the trailing edge. Fixing collocation point placement effectively sets circulation. Therefore, control-point/influence-point positioning can be critical to zero-thickness lifting-surface methods. An important feature of the method described in this paper is its insensitivity to collocation point location.

Smoothed Doublets

Before proceeding to develop the ANM method for lifting-surface theory, the smoothed doublet, which is the basic building block of the method, is described. The concept of smoothing singularities has its roots in the field of computational vortex dynamics.[8–11,19] Because of the singular nature of many types of numerical vortex elements, instabilities occur in the solution process and can adversely affect numerical results. To address this problem, smoothing functions and convolution integrals have been introduced to help remove the nonphysical large gradients from the problem, thereby encouraging convergent solutions.[8–10,20–22]

The following discussion describes the development of smoothed doublets as a natural extension of the concepts used in computational vortex dynamics. A distribution of doublets can be shown mathematically to be equivalent to distributions of vortices. The ideas developed in this section can be extended to include the fundamental solutions of both the acoustic wave equation[23] and the convective wave equation.[24]

A smoothed doublet is analogous to the familiar singular potential doublet, except that there is a spatial distribution of doublet strength density.[23] Smoothed doublets, sketched in Figs. 1 and 2, are nonsingular everywhere, and, away from the distribution region, they have the same behavior as an equivalent singular doublet with the same aggregate strength. Please note, that Figs. 1 and 2 are for illustration purposes only, and in fact, the smoothed doublet exhibits a far more complex shape than that sketched in the figures. Smoothed doublets can be constructed from singular doublets by a simple transformation of the radial variable,

$$R \to R_s = \sqrt{(x-\xi)^2 + (y-\eta)^2 + (z-\zeta)^2 + r_c^2}$$

where r_c is an additional smoothing length scale. This construction can be done so that a velocity potential exists.[23] Overlapping

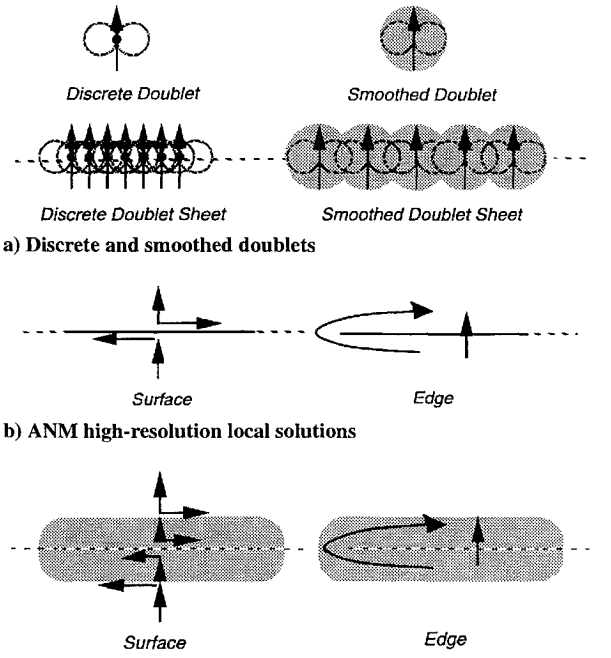

Fig. 2 Building blocks of the ANM solution.

discrete smoothed doublets have been shown to approximate a continuous distribution accurately. In three dimensions, the potential for a smoothed doublet can be written

$$\varphi_{\text{doublet}_{\text{smooth}}} = -(\mu/4\pi)\left(R/R_s^3\right)\cos\theta \tag{5}$$

where μ is the net doublet strength and θ is the angle between the doublet orientation vector and the vector between the field point at (x, y, z) and doublet origin at (ξ, η, ζ). The associated velocity field can be found by differentiation. In Cartesian coordinates, for a doublet at the origin oriented in the $\hat{e}_k$ direction, this gives

$$\begin{aligned} \boldsymbol{u} = -\frac{\mu}{4\pi}\Bigg\{ & \left[\frac{-3xz}{\left(x^2+y^2+z^2+r_c^2\right)^{\frac{5}{2}}}\right]\hat{e}_i \\ & + \left[\frac{-3yz}{\left(x^2+y^2+z^2+r_c^2\right)^{\frac{5}{2}}}\right]\hat{e}_j \\ & + \left[\frac{x^2+y^2-2z^2+r_c^2}{\left(x^2+y^2+z^2+r_c^2\right)^{\frac{5}{2}}}\right]\hat{e}_k \Bigg\} \end{aligned} \tag{6}$$

where the partial derivative was taken with respect to z.

Equations (5) and (6) are smooth functions, and no longer singular. There is a smooth spatial distribution of doublet strength concentrated about the origin. As a result, the potential or velocity approaches a constant value as $r \to 0$. Note, however, that as r gets large, namely $r \gg r_c$, the values tend quickly toward the potential value without smoothing. In the limit when $r_c \to 0$, the nonsmoothed potential and velocity are recovered. The smoothed functions can be interpreted as convolutions of the nonsmooth singular results with a suitable smoothing function.[20] Note that the radial smoothing used is fully self-consistent, and therefore, two-dimensional results can be simply obtained in closed form by integration of the three-dimensional results.

The smoothing operation takes a discrete singularity, a doublet in this case, and replaces it with a continuous distribution having the same net strength and the same far-field behavior. As a result, the region over which the singularity is distributed is no longer divergence free, although it is irrotational. The governing equation is then an inhomogeneous Laplacian equation with a distributed source/sink distribution on the right-hand side. Because a doublet

was smoothed to make this distribution, the distributed terms look like a source distribution above the axis and a sink distribution below. However, this distribution also can be interpreted as a spatial distribution of doublets.

When the ANM solution procedure separates the problem into local and global parts, as illustrated in Fig. 1 and the associated discussion, the global solution and the local matching solution are not divergence free, and do not satisfy the homogeneous Laplacian equation, but rather a Poisson equation (the inhomogeneous Laplacian equation). When the composite solution is constructed for this linear problem, the distributed source/sink effects from the global and matching solutions cancel (after all, their equal and opposite nature was the basis for decomposing the solution in Fig. 1), and the composite solution does satisfy the homogeneous version of Laplace's equation.

This part of the solution procedure, which involves a decomposition by adding and subtracting smoothed singularities, is actually one of the keys to how the method works. Understanding the role of smoothing is a subtle point, especially because the smoothing cancels out in the final answer. This process is one of the real innovations of the ANM method.

ANM Aerodynamics

A distribution of smoothed doublets, as given by Eq. (5), is added to and subtracted from Eq. (3), with no net change in the equation, giving

$$\varphi(p) = \left[\frac{1}{4\pi}\iint_{S_b+S_w}\left\{\mu_\omega\left[\frac{\partial}{\partial n}\left(\frac{1}{R_s}\right)\right]\right\}\mathrm{d}S + \left(\frac{1}{4\pi}\iint_{S_b+S_w}\left\{\mu_\omega\left[\frac{\partial}{\partial n}\left(\frac{1}{r}\right)\right]\right\}\mathrm{d}S - \frac{1}{4\pi}\iint_{S_b+S_w}\left\{\mu_\omega\left[\frac{\partial}{\partial n}\left(\frac{1}{R_s}\right)\right]\right\}\mathrm{d}S\right)\right] \tag{7}$$

Combining the two integrals in the second term on the right-hand side and taking the normal derivative gives

$$v_n(p) = \boldsymbol{n}\cdot\left(\frac{1}{4\pi}\iint_{S_b+S_w}\left\{\mu_\omega\nabla\left[\frac{\partial}{\partial n}\left(\frac{1}{R_s}\right)\right]\right\}\mathrm{d}S + \frac{1}{4\pi}\iint_{S_b+S_w}\left\{\mu_\omega\nabla\left[\frac{\partial}{\partial n}\left(\frac{1}{r}\right)-\frac{\partial}{\partial n}\left(\frac{1}{R_s}\right)\right]\right\}\mathrm{d}S\right) \tag{8}$$

Notice that the integrand in the second term on the right-hand side of Eq. (8) becomes negligible when $r \gg r_c$, because $R_s \to r$ and the value of the smooth doublet kernel function approaches that of the singular kernel function, and they asymptotically cancel each other. The contribution of this integral becomes significant only when $r = \mathcal{O}(r_c)$.

On the surface $S_b + S_w$, where v_n is specified, there is a small region S_{r_c} about p where $r = \mathcal{O}(r_c)$. Note, however, that most of the contribution to the integral comes from the region S_{r_c} immediately about p. Therefore, the bounds of integration can be modified such that the integration is done on any surface S_{mod} that contains S_{r_c}, without changing the final result.

Because of the local nature of the integral over S_{mod}, a series expansion about p can be written for the doublet strength density:

$$\mu_\omega(\boldsymbol{p}+\Delta\boldsymbol{r}) = \mathcal{F}(\Delta\boldsymbol{r})\sum_{k=0}^{\infty}\frac{1}{k!}(\Delta\boldsymbol{r}\cdot\nabla)^k\mu_\omega(\boldsymbol{p}) \tag{9}$$

where $\Delta\boldsymbol{r}$ is the vector change in position on the surface, $\boldsymbol{p}$ is the vector location of p, and $\mathcal{F}(\Delta\boldsymbol{r})$ is a weighting function discussed in the next section. Essentially, $\mathcal{F}(\Delta\boldsymbol{r})$ is included because the doublet strength density may be nonanalytical approaching the edges of the lifting surface. Only the first few terms in the series are necessary; however, at this point the entire series is retained for completeness. Substituting the series expression into Eq. (8), and changing the bounds of integration on the second integral from $S_b + S_w$ to S_{mod} gives

$$v_n(p) = \boldsymbol{n}\cdot\left(\frac{1}{4\pi}\iint_{S_b+S_w}\left\{\mu_\omega\nabla\left[\frac{\partial}{\partial n}\left(\frac{1}{R_s}\right)\right]\right\}\mathrm{d}S + \frac{1}{4\pi}\iint_{S_{\mathrm{mod}}}\left\{\mathcal{F}\sum_{k=0}^{\infty}\frac{1}{k!}(\Delta\boldsymbol{r}\cdot\nabla)^k\mu_\omega(\boldsymbol{p}) \times\nabla\left[\frac{\partial}{\partial n}\left(\frac{1}{r}\right)-\frac{\partial}{\partial n}\left(\frac{1}{R_s}\right)\right]\right\}\mathrm{d}S\right) \tag{10}$$

This can then be rewritten as

$$v_n(p) = \boldsymbol{n}\cdot\left[\frac{1}{4\pi}\iint_{S_b+S_w}\left\{\mu_\omega\nabla\left[\frac{\partial}{\partial n}\left(\frac{1}{R_s}\right)\right]\right\}\mathrm{d}S + \sum_{k=0}^{\infty}\left(\varphi_k^{\mathrm{local}}(p) - \frac{\mathcal{F}}{4\pi}\iint_{S_{\mathrm{mod}}}\left\{\frac{1}{k!}(\Delta\boldsymbol{r}\cdot\nabla)^k\mu_\omega(\boldsymbol{p}) \times\nabla\left[\frac{\partial}{\partial n}\left(\frac{1}{R_s}\right)\right]\right\}\mathrm{d}S\right)\right] \tag{11}$$

where

$$\varphi_k^{\mathrm{local}}(p) = \frac{\mathcal{F}}{4\pi}\iint_{S_{\mathrm{mod}}}\left\{\frac{1}{k!}(\Delta\boldsymbol{r}\cdot\nabla)^k\mu_\omega(\boldsymbol{p})\nabla\left[\frac{\partial}{\partial n}\left(\frac{1}{r}\right)\right]\right\}\mathrm{d}S \tag{12}$$

$\varphi_k^{\mathrm{local}}$ is the local potential, and in Eq. (12) it is written in terms of an integral over the surface S_{mod}. This integral represents a family of simple flow solutions to Laplace's equation, as shown in Fig. 3, which can be found by separation of variables. As such, the explicit integration of Eq. (12) is not required. Eq. (11) is the fundamental integral equation of the boundary element method. In two dimensions, Eq. (11) becomes

$$v_n^{2D}(p) = -\boldsymbol{n}\cdot\left(\frac{1}{2\pi}\int_{\Gamma_b+\Gamma_w}\left\{\mu_{2D}\nabla\left[\frac{\partial}{\partial n}(\ell_v\hat{R}_s)\right]\right\}\mathrm{d}S + \sum_{k=0}^{\infty}\frac{\mu_{2D}^{(k)}(p)}{k!}\left\{\varphi_k^{\mathrm{local}}(p) - \frac{\mathcal{F}}{2\pi}\int_{\Gamma_{\mathrm{mod}}}(x-p)^k \times\nabla\left[\frac{\partial}{\partial n}(\ell_v\hat{R}_s)\right]\mathrm{d}S\right\}\right) \tag{13}$$

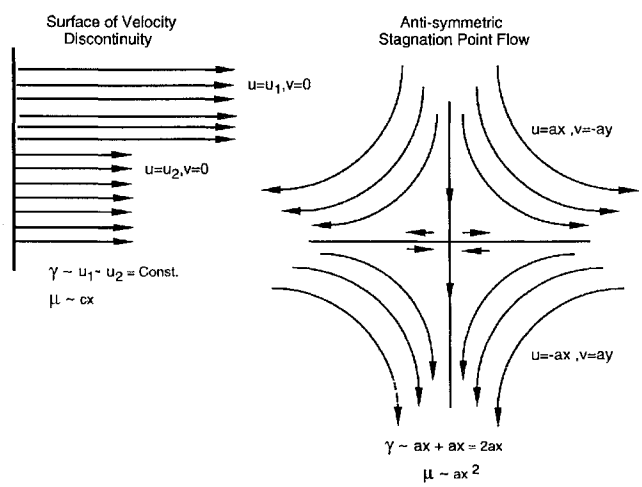

Fig. 3 Examples of simple flow solutions to Laplace's equation, corresponding to nonsmoothed linear and quadratic doublet distributions.

where

$$\varphi_k^{\text{local}}(p) = \frac{\mathcal{F}}{2\pi} \int_{\Gamma_{\text{mod}}} (x - p)^k \nabla \frac{\partial}{\partial n}(\ell_n \hat{r})\, \mathrm{d}S \tag{14}$$

Again φ_k^{local} represents simple flow solutions to Laplace's equation, the hat notation denotes two dimensions, Γ_{mod} is a contour that contains Γ_{r_c}, and the series expansion is taken about p.

Note that, if the point p is not on the surface $S_B + S_w$, Eqs. (11–13) are integral representations of the normal velocity field, in terms of the normal velocity field on the surface $S_b + S_w$. If the point p is on S_b, Eqs. (11–13) become inhomogeneous Fredholm integral equations of the first kind, relating the known normal velocity v_n to the unknown values of μ_ω on S_b, where the values on S_w can be explicitly determined from the values on S_b. At this point, the advantage of using Eqs. (11–13) may not be clear; however, it will be shown that, because of their smooth nature, these equations are advantageous for numerical implementation.

Examining the terms in Eq. (11) in greater detail reveals the relationship between the original problem, Eq. (3), and the problem cast in terms of ANM. The ANM methodology breaks the problem up into global and local constituent parts. The first term on the right-hand side of the equation embodies smoothed global effects, ultimately treated numerically, whereas the second term is a local correction that can be found analytically.

Figure 1 shows a schematic of the ANM decomposition of the original linear problem. As a first step, equivalent smoothed singularity distributions are added to and subtracted from the original problem, as given in Eq. (7). Because these smoothed distributions exactly cancel, the net result is unchanged. However, as shown in Eq. (7), the singularity distributions also can be regrouped. The first smoothed singularity distribution, the first term on the right-hand side of Eq. (7), can be viewed as the low-resolution smoothed global problem, and represented by discrete overlapping smoothed doublets, given by Eq. (5), as shown in Fig. 1. The second (original) distribution and the third (smoothed) distribution can be combined, as in Eq. (8). When this is done, these two distributions always cancel at points away from the point of evaluation, because their far-field behavior is the same. Thus, only the local behavior of these distributions ultimately matters. For convenience, they can be evaluated as if they are part of an infinite sheet (or a semi-infinite sheet if near an edge). Using a Taylor-series expansion of the singularity strength distribution in this local region, Eq. (9), it can be shown that these local solutions can be expressed in terms of simple flowfields obtained from the governing equation by separation of variables.

An interesting feature of the ANM composite solution, given by Eqs. (11–13), is that all of its constituent parts are functionally smooth. In fact, it is only vaguely reminiscent of a traditional panel method. The surface $S_b + S_w$ of Eq. (3) is no longer discretely approximated by a contiguous set of panels but rather by a discrete distribution of overlapping smoothed doublets. Therefore, the idea of a surface of contiguous panels exists only with regard to the spacing between adjacent smoothed doublets. The authors believe that this smoothness leads to accurate, rapidly converging numerics. In addition, the analytical aspects of the problem are well defined and well behaved. The traditional problems associated with discretizing a singular integral equation to obtain a numerical solution are avoided. In contrast to traditional discretized calculations, there is no ambiguity as to whether local averages or point values of variables, such as pressure, are being computed on panels. ANM computes local values of variables, and even handles singular behavior at edges in a formal manner that allows singularity strength to be determined. Sources of error are quantifiable, and there is a procedure for extending the method to higher-order accuracy. The local solutions, because of their nature, satisfy the Kutta condition regardless of control-point/influence-point positioning.

ANM Local Correction

The local correction is based on the second term on the right-hand side of Eq. (11), which represents the difference between a distribution of conventional doublets and smoothed doublets. The difference between these distributions cancels far away; therefore, the far-field shape and behavior are unimportant, allowing for simplification in the evaluation of the integral. The domain of integration only needs to be geometrically correct immediately about p. In particular, when considering a flat surface, for convenience, the bounds of integration can be taken to infinity. The integration is done on an infinite flat surface (a contour in two dimensions) with p located at the origin, given by

$$\mathcal{L}_w = \boldsymbol{n} \cdot \left\{ \frac{1}{4\pi} \int_{-\infty}^{\infty} \int_{-\infty}^{\infty} \mathcal{F} \sum_{n=0}^{\infty} \frac{1}{n!} (\Delta \boldsymbol{r} \cdot \nabla)^n \mu_\omega(\boldsymbol{p}) \times \nabla \left[\frac{\partial}{\partial n}\left(\frac{1}{r}\right) - \frac{\partial}{\partial n}\left(\frac{1}{R_s}\right) \right] \mathrm{d}S \right\} \tag{15}$$

where $\mathcal{L}_w$ denotes the net local correction. Any effects from the far field will cancel, leaving only the local difference between the smoothed and conventional distributions. Therefore, in practice, only the first few terms in the series need to be retained. Special consideration is made for edges, because of the additional length scale that measures from the tip of the edge to p. A point P is determined to be close to the edge if it is a distance of $\mathcal{O}[r_c]$ from the edge. In this case, the integration is taken over semi-infinite bounds along the edge coordinate direction, starting at the edge, where p is located a distance l inboard of the edge:

$$\mathcal{L}_w^{\text{edge}} = \boldsymbol{n} \cdot \left\{ \frac{1}{4\pi} \int_{0}^{\infty} \int_{-\infty}^{\infty} \mathcal{F} \sum_{n=0}^{\infty} \frac{1}{n!} (\Delta \boldsymbol{r} \cdot \nabla)^n \mu_\omega(\boldsymbol{p}) \times \nabla \left[\frac{\partial}{\partial n}\left(\frac{1}{r}\right) - \frac{\partial}{\partial n}\left(\frac{1}{R_s}\right) \right] \mathrm{d}S \right\} \tag{16}$$

The contribution of the distribution of conventional doublets in Eqs. (15) and (16), the first term in the square brackets, is called the high-resolution local solution. It contains the details of the local flow structure, including the local gradients. Looking specifically at this part of the integral, it can easily be shown that the high-resolution local solution consists of exact solutions to Laplace's equation on an infinite or semi-infinite domain. This is because it consists of integral distributions of free-space Green's functions with varying strength distributions given by the terms in the series, which explicitly satisfy the boundary conditions. As such, by considering the terms in the Taylor series of the doublet strength distribution in Eqs. (15) and (16), the flowfield about a control point can be deduced in terms of simple exact solutions to Laplace's equation on an infinite domain, shown in Fig. 3. Note that the antisymmetric stagnation-point flow in Fig. 3 corresponds to a linear vortex distribution on a doubly infinite straight contour. This flow requires careful evaluation because of the existence of an eigensolution at infinity. The eigensolution is canceled exactly by the existence of an eigensolution in the matching solution of opposite sign.

Therefore, using the Taylor series as a guide, solutions to Laplace's equation can be found that match the power of each term in the series and represent the integrated singular Green's function distributions given in Eqs. (15) and (16). As noted earlier, the series can be truncated at any desired accuracy; however, depending on S_{mod}, care must be taken to ensure that the resulting integrals are uniformly convergent. In the present implementation, the series was truncated after the quadratic terms.

The contribution of the distribution of smoothed doublets in Eqs. (15) and (16), the second term in the square brackets, is called the matching solution. It cancels the global solution locally, and the local high-resolution solution globally, thereby asymptotically matching the global solution to the local high-resolution solution. The matching solution is precisely a smoothed version of the high-resolution local solution.

The smoothing, as shown in Fig. (2), can be done by any suitable means; however, a technique called the split-sheet analogy is effective. This approach is based on the observation that the smoothing process is similar to viewing a singular solution at an offset location. In particular, consider the smoothed doublet velocity field of Eq. (6)

when viewed in the $z = 0$ plane, which is the surface on which the downwash is evaluated. This expression can be shown to be the same as that for a discrete source and sink displaced a distance r_c above and below the $z = 0$ plane, respectively, provided the doublet strength and source strength are related as $\mu = 2r_c\sigma$. It follows that a sheet of smoothed doublets on $z = 0$ can be replaced by corresponding sheets of discrete sources and sinks, offset above and below $z = 0$ by distance r_c. For the calculation of downwash, smoothing a doublet sheet is equivalent to splitting the doublet sheet into its constituent source and sink sheets displaced an appropriate amount. This approach leads to a simple way to construct smoothed local solutions using separation of variables. Because the local solutions can be interpreted basic flows obtained by separation of variables, as shown in Fig. (3), the smoothed local solutions used for matching also can be obtained in a similar manner. However, these flows must be associated with source/sink surfaces, rather than doublet surfaces. Furthermore, the downwash associated with these surfaces must be evaluated at positions offset above and below the surfaces a distance r_c. This approach, which has been verified by other means (direct integration of the kernel function), is particularly straightforward and insightful.

The net local correction is the difference between the high-resolution local solution and the matching solution, the terms in the square brackets of Eqs. (15) and (16). For a flat surface with coordinates (x, y), the net local correction $\mathcal{L}_w$, at the point (x_1, y_1), in terms of upwash, is given by

$$\mathcal{L}_w = \boldsymbol{n} \cdot \left(\frac{1}{4\pi} \int_{-\infty}^{\infty}\int_{-\infty}^{\infty} \left\{ \mu_\omega(x_1, y_1) + (x - x_1)\frac{\partial \mu_\omega}{\partial x} + (y - y_1)\frac{\partial \mu_\omega}{\partial y} + \frac{1}{2!}\left[(x - x_1)^2 \frac{\partial^2 \mu_\omega}{\partial x^2} + 2(x - x_1)(y - y_1)\frac{\partial^2 \mu_\omega}{\partial x \partial y} + (y - y_1)^2 \frac{\partial^2 \mu_\omega}{\partial y^2} \right] \right\} \times \nabla\left[\frac{\partial}{\partial n}\left(\frac{1}{r}\right) - \frac{\partial}{\partial n}\left(\frac{1}{R_s}\right) \right] \mathrm{d}S \right)$$

$$= -\frac{\mu_\omega}{2r_c} + \frac{r_c}{4}\left(\frac{\partial^2 \mu_\omega}{\partial x^2} + \frac{\partial^2 \mu_\omega}{\partial y^2} \right) \tag{17}$$

where the truncated Taylor series has been substituted into Eq. (15) and $\mathcal{F}$ is taken as unity. Only the even terms in x or y contribute to the integral.

It is documented in the literature[25,26] that, for two-dimensional subsonic flow about edges, there is a $\frac{1}{2}$-power singularity in the tangential velocity component just inboard of an edge. Therefore, at an edge in two dimensions, or sufficiently close to an edge in three dimensions, the doublet strength distribution can be expected to be expanded in powers of $\frac{1}{2}$:

$$\mu_{\mathrm{edge}}(x) = c_0 x^{\frac{1}{2}} + c_1 x^{\frac{3}{2}} + \mathcal{O}\left(x^{\frac{5}{2}}\right) \tag{18}$$

where c_0 and c_1 are arbitrary constants.

In three dimensions, Eq. (18) can be thought of as the leading order term in an asymptotic expansion, because, very close to an edge, the two-dimensional terms dominate the three-dimensional terms in the solution. This can be demonstrated with as simple perturbation expansion about the edge. Trouble could possibly arise at the wingtip corners, where two edges are present. Here, however, the flowfield can be modeled with conical flow solutions.[25,27] Numerical experimentation has shown that the conical flow solutions are not required for sufficient accuracy. If, however, higher accuracy is needed, higher-order wingtip corner solutions can be constructed from conical flow solutions.

Therefore, the weighting function $\mathcal{F}$ in Eq. (9) should be $\sqrt{(\Delta r)}$ for the edge panels (unity elsewhere). As mentioned earlier, this is because the doublet strength distribution becomes nonanalytical at the edge. At any point l on the surface near the edge, c_0 and c_1 can be determined in terms of the derivative of Eq. (18), ignoring terms of $\mathcal{O}(x^{3/2})$, such that

$$c_0 = \frac{3}{2}\frac{\mu_{\mathrm{edge}}(l)}{\sqrt{l}} - \sqrt{l}\frac{\mathrm{d}}{\mathrm{d}x}[\mu_{\mathrm{edge}}(x)]_{x=l}$$

$$c_1 = \frac{1}{\sqrt{l}}\frac{\mathrm{d}}{\mathrm{d}x}[\mu_{\mathrm{edge}}(x)]_{x=l} - \frac{1}{2}\frac{\mu_{\mathrm{edge}}(l)}{l^{\frac{3}{2}}} \tag{19}$$

The series expansion of the doublet distribution for an edge, Eq. (18), now can be written in terms of the doublet strength density and its derivative as

$$\mu_{\mathrm{edge}}(x) = \left[\frac{3}{2}\frac{\mu_{\mathrm{edge}}(l)}{\sqrt{l}} - \sqrt{l}\frac{\mathrm{d}}{\mathrm{d}x}[\mu_{\mathrm{edge}}(x)]_{x=l} \right] x^{\frac{1}{2}} + \left[\frac{1}{\sqrt{l}}\frac{\mathrm{d}}{\mathrm{d}x}[\mu_{\mathrm{edge}}(x)]_{x=l} - \frac{1}{2}\frac{\mu_{\mathrm{edge}}(l)}{l^{\frac{3}{2}}} \right] x^{\frac{3}{2}} \tag{20}$$

where x can be any coordinate direction inboard of an edge. After substitution of Eq. (20) into Eq. (16), and evaluation [similar to Eq. (17)], the corresponding correction in terms of upwash for edge panels is

$$\mathcal{L}_w^{\mathrm{edge}}(x) = -\left[(c_0/2r_c)(R_{r_c})^{\frac{1}{2}} \cos(\theta/2) + (c_1/2r_c)(R_{r_c})^{\frac{3}{2}} \cos(3\theta/2) \right] \tag{21}$$

where x is the coordinate inboard of the edge, $R_{r_c} = \sqrt{(x^2 + r_c^2)}$, and $\theta = \arctan(r_c/x)$.

Numerical Results

Most modern panel methods solve the Prandtl–Glauert equation for steady subsonic flow.[1] With this consideration, test calculations were done to better understand and validate the novel methodology. Well-understood aerodynamic problems with generally accepted numerical results were examined. The following section presents the results for the ANM analysis of steady incompressible flow over a lifting flat-plate airfoil in two dimensions, and a lifting rectangular thin wing of finite span in three dimensions. The analysis is easily extendable to include steady compressible flow by implementing a Prandtl–Glauert[12] or Göthert[12] transformation, on the global, local, and matching solutions.

Figures 4 and 5 show the results for doublet strength density and coefficient of pressure along a flat-plate airfoil at 5-deg angle of incidence. The pressure coefficient calculation is done using the linearized form of the Bernoulli equation. The calculation used 20 discrete smoothed doublets along the chord because integrated panels are not necessary; the spacing between doublets was 5% of the total chord, and the smoothing length scale r_c was 1.3 times the panel length l, or 0.065 times the total chord length c. Unlike traditional panel methods, control points where the boundary conditions are satisfied and influence points where the discrete smoothed doublets are located were placed on top of each other. The wake also is modeled with smoothed discrete doublets that continue off of the lifting surface with the strength of the last doublet along the chord

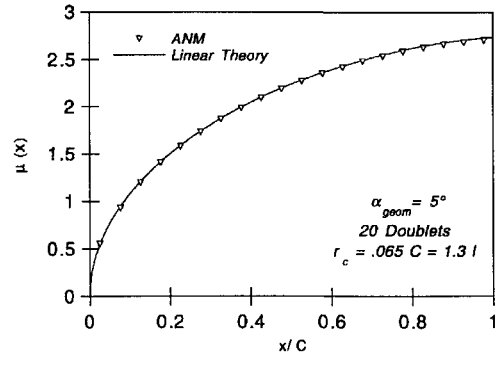

Fig. 4 Doublet strength density vs chordwise position for a flat-plate airfoil. Control points and influence points are superimposed at locations indicated by the data symbols.

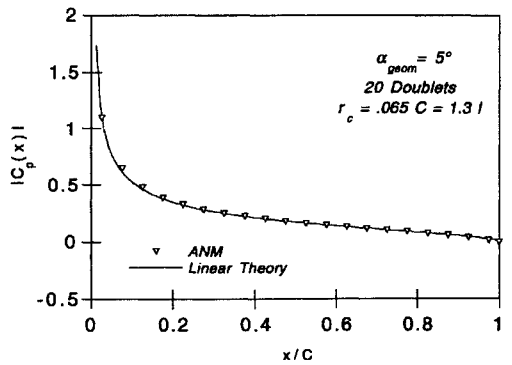

Fig. 5 Coefficient of pressure vs chordwise position for a flat-plate airfoil. Control points and influence points are superimposed.

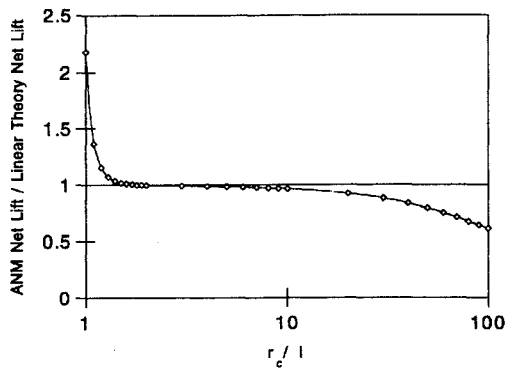

Fig. 6 Solution overlap region for an ANM net lift calculation (α_{geom} = 5/deg, 20 doublets, r_c = 0.065c), $c_p \rightarrow \frac{1}{2}$ $i_p \rightarrow \frac{1}{2}$.

(at each spanwise location in three dimensions). The agreement between ANM and linear small disturbance theory is very good. The circulation distribution is calculated from the doublet strength distribution. The values of doublet strength density and circulation along the leading-edge panel can be solved for directly, using the multiplicative constants c_0 and c_1.

The smoothing length scale r_c controls the amount of smoothing used. It is desirable to make the global solution as smooth as possible, by removing any large spatial gradients, thereby improving numerical convergence and ultimately reducing any dependencies on control-point/influence-point location. If too much smoothing is used, however, the global and local solutions do not match properly, and the solution will degrade. Furthermore, if the smoothing radius is too small, the global solution will no longer be smooth, and will not properly match the local solution. Then, the solution will degrade because of the discreteness errors typical of a lower-order panel method, and the influence of large spatial gradients.

There is a range of smoothing that provides the best global–local solution match, such that there is a mathematical overlap between the global and local solutions. The smoothing length scale should be on the order of the spacing between smoothed doublets in the global solution. Typically, values of 1.2–1.8 times the doublet spacing work well. Figure 6 shows the solution overlap for the preceding calculation, shown in Figs. 4 and 5. In Fig. 6 the net ANM lift is normalized by the net lift calculated by linear theory, and plotted as a function of the smoothing length scale r_c normalized by the distance between smoothed doublets in the global solution l. The control points are collocated with the influence points in the calculation.

Figure 7 shows the chordwise circulation distribution for a flat plate at 5-deg angle of incidence. The smoothing length scale used in the calculation is 1.3 times the smoothed doublet spacing (0.065 of the total chord length), 20 smoothed doublets were used in the calculation, and the control-point locations were variable (indicated in the legend as a fraction of the doublet spacing, influence-point location first). Note that the solution is almost independent of control-point/influence-point placement. In fact, for one case, the control points are actually in front of the influence points.

The calculations shown in Fig. 7 would be difficult, if not impossible, with traditional zero-thickness lifting-surface methods.[18,28–31]

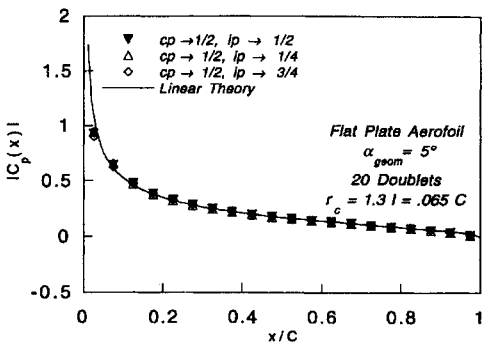

Fig. 7 Coefficient of pressure calculated for various control-point locations, with a fixed influence-point location.

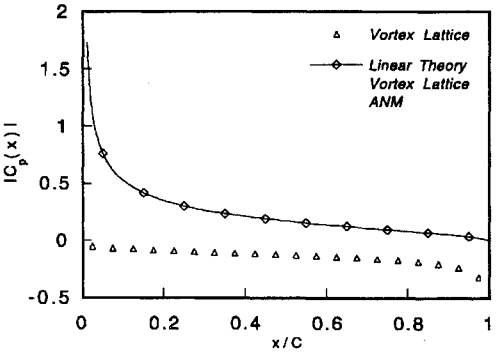

Fig. 8 Comparison between ANM and vortex lattice calculations; influence points are at the center of each panel, and control points are at the quarter position of each panel.

This is because of the hypersingular kernel function found in the integral equation used by these methods. The problem arises from the necessity of taking the normal derivative of the velocity potential induced by a distribution of doublets. To illustrate this point, Fig. 8 shows a comparison between an ANM calculation of the pressure coefficient along the chord of a flat-plate airfoil at a nominal angle of attack, and a comparable vortex lattice calculation. The calculation was done using 20 smoothed doublets, and 20 vortex panels. The influence points are not at the $\frac{1}{4}$ chord of each panel, but rather at the center, and the control points are at the $\frac{1}{4}$ chord of each panel, rather than the $\frac{3}{4}$ chord. The vortex lattice result uniformly converges to the incorrect result. Note, however, if the influence points are at the $\frac{1}{4}$ chord of each panel, and the control points are at the $\frac{3}{4}$ chord of each panel, the vortex lattice method and ANM both converge to the correct result.

If we consider the situation when control points and influence points are at the same location, catastrophic errors occur in the vortex lattice influence-coefficient matrix because of numerical divergence, resulting in nonconvergent solutions. This is rather unfortunate, because placing influence points and control points at the same location only requires one geometric point per computational panel, and therefore simplifies the computation needed. In the future, when the method is extended to include more complex geometries, this will offer a large level of simplification.

To illustrate the convergence characteristics of ANM, Fig. 9 shows calculations for a flat-plate airfoil at 5-deg incidence angle with various numbers of smoothed doublets used in the calculation. In the calculation, the smoothing length scale was 1.3 times the spacing between smoothed doublets. The calculation is nearly converged with only five panels.

Figure 10 shows the spanwise component of the surface vortex distribution at the midspan of an aspect-ratio-5 wing, at 5-deg incidence. The calculation was done with a 10 × 50 grid of smoothed doublets (50 along the span, 10 along the chord). The smoothing length scale was 1.5 times the spacing between smoothed doublets along the chord, and the control points were collocated with influence points at the smoothed doublet positions. ANM accurately captures the leading-edge singularity and the dropoff of the chordwise component of the vortex distribution at the trailing edge. The calculation compares well to the vortex lattice calculation. Note,

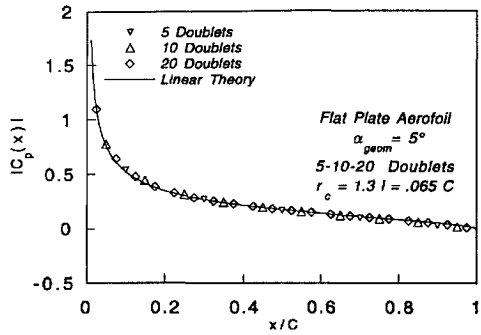

Fig. 9 Coefficient of pressure for various numbers of doublets.

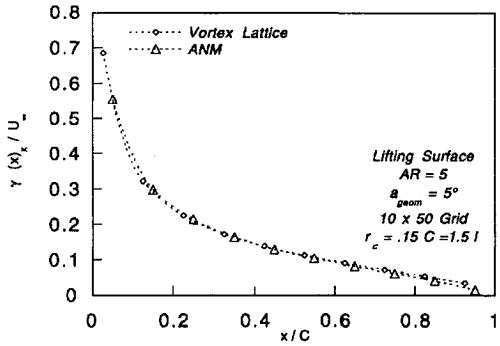

Fig. 10 Circulation distribution along the midspan of an aspect-ratio-5 wing (α_{geom} = 5 deg, 10 × 50 grid, r_c = 0.15 chord).

however, that unlike the vortex lattice calculation, the ANM solution can be calculated at any point along the chord near the leading edge, not just at the specified influence points. Therefore, there are no problems with numerical resolution at the leading edge. In compressible unsteady flow, this can become very important for acoustic radiation calculations.[23,24]

Concluding Remarks

A boundary element method based on smoothed fundamental solutions to Laplace's equation has been developed and applied successfully to linear aerodynamics problems. The formulation is based on a technique called ANM, which offers a fresh point of view on classic lifting-surface theory, by solving the problem with a fundamentally different mean. The ANM approach breaks the problem up into global and local constituent problems that are defined by the physical length scales of the problem and an additional smoothing length scale.

ANM offers a unified aerodynamic methodology without the traditional problems associated with the numerical solution of singular integral equations. The ANM boundary element formulation leads to accurate solutions, rapid numerical convergence, and is free from the ambiguity present in many traditional zero-thickness lifting-surface methods. Additionally, ANM does not have rigid rules on influence-point/control-point location, and therefore is suitable for hybrid fluid–structure calculations requiring a matching computational grid.

The methodology, free from stringent rules on control-point/influence-point location, is therefore less restrictive. ANM offers clear advantages for analysis of complex geometric configurations, and for calculations that involve interfacing with some other sort of numerical computation, such as a structural analysis code.

In practice, ANM is a simple methodology that offers high-resolution aerodynamic calculations in the framework of a unified aerodynamic theory. In the future, one can envision the method being applied to a multitude of aerodynamic problems, including the design and analysis of advanced aerodynamic configurations. The methodology, free from stringent rules on control-point/influence-point location, is therefore less restrictive than many present methods.

Acknowledgments

This work was supported by a Graduate Student Researchers Program Fellowship from the NASA Langley Research Center with Thomas F. Brooks serving as technical monitor.

References

[1]Erickson, L. L., "Panel Methods—An Introduction," NASA, TP-2995, 1990.

[2]Lifanov, I. K., and Polonskii, I. E., "Proof of the Numerical Method of Discrete Vortices for Solving Singular Integral Equations," *Journal of Applied Mathematics and Mechanics*, Vol. 39, No. 4, 1975, pp. 742–746.

[3]Johnson, F. T., and Rubbert, P. E., "Advanced Panel-Type Influence Coefficient Methods Applied to Subsonic Flows," AIAA Paper 75-50, Jan. 1975.

[4]Johnson, F. T., Rubbert, P. E., and Ehlers, F. E., "A Higher Order Panel Method for General Analysis and Design Applications in Subsonic Flow," *5th International Conference on Numerical Methods in Fluid Dynamics* (Enschede, The Netherlands), Springer–Verlag, Berlin, 1976, pp. 247–253.

[5]Johnson, W., "Recent Developments in Rotary-Wing Aerodynamic Theory," *AIAA Journal*, Vol. 24, No. 8, 1986, pp. 1219–1244.

[6]Margason, R. J., "Subsonic Panel Methods—A Comparison of Several Production Codes," AIAA Paper 85-0280, Jan. 1985.

[7]Landahl, M. T., and Stark, J. E., "Numerical Lifting Surface Theory—Problems and Progress," *AIAA Journal*, Vol. 6, No. 1, 1968, pp. 2049–2060.

[8]Miller, W., "Analytical/Numerical Matching and Periodic Inversion: Two Advances in Free Wake Analysis," Ph.D. Thesis, Dept. of Mechanical Engineering and Materials Science, Duke Univ., Durham, NC, 1990.

[9]Epstein, R. J., "Improved Efficiency in Free Vortex Problems Using Analytical/Numerical Matching and Solution Pyramiding," M.S. Thesis, Dept. of Mechanical Engineering and Materials Science, Duke Univ., Durham, NC, 1991.

[10]Bliss, D. B., and Miller, W. O., "Efficient Free Wake Calculations Using Analytical/Numerical Matching," *Journal of the American Helicopter Society*, Vol. 38, No.2, 1993, pp. 878, 879.

[11]Epstein, R. J., and Bliss, D. B., "Free Vortex Calculations Using Analytical/Numerical Matching with Solution Pyramiding," *AIAA Journal*, Vol. 33, No. 5, 1995, pp. 894–903.

[12]Ashley, H., and Landahl, M., *Aerodynamics of Wings and Bodies*, Dover, New York, 1965, Chap. 7.

[13]Kellogg, O. D., *Foundations of Potential Theory*, Dover, New York, 1953, Chap. 2.

[14]Baker, B., and Copson, E., *Mathematical Theory of Huygens' Principle*, Chelsea Publishing, New York, 1987, Chap. 1.

[15]Katz, J., and Plotkin, A., *Low Speed Aerodynamics, from Wing Theory to Panel Methods*, McGraw–Hill Series in Aeronautical and Aerospace Engineering, McGraw–Hill, New York, 1991, Chap. 3.

[16]Lamb, H., *Hydrodynamics*, Dover, New York, 1962, Chap. 3.

[17]Mangler, K. W., and Smith, J. H. B., "Behavior of the Vortex Sheet at the Trailing Edge of a Lifting Edge Wing," *Aeronautical Journal*, Vol. 74, Nov. 1970, pp. 906–908.

[18]Albano, E., and Rodden, W., "A Doublet-Lattice Method for Calculating Lift Distributions on Oscillating Surfaces in Subsonic Flows," *AIAA Journal*, Vol. 7, No. 2, 1969, pp. 279–285.

[19]Anderson, C., and Greengard, C. (eds.), *Vortex Methods*, Lecture Notes in Mathematics, Springer–Verlag, New York, 1988.

[20]Beale, J. T., and Majda, A., "High Order Accurate Vortex Methods with Explicit Velocity Kernels," *Journal of Computational Physics*, Vol. 58, No. 2, 1985, pp. 188–208.

[21]Rosenhead, L., "The Spread of Vorticity in the Wake Behind a Cylinder," *Proceedings of the Royal Society of London Series A: Mathematical and Physical Sciences*, Vol. 127, 1930, pp. 590–612.

[22]Widnall, S. E., and Bliss, D. B., "Theoretical and Experimental Study of the Stability of a Vortex Pair," *Aircraft Wake Turbulence and Its Detection*, edited by J. Olson, A. Goldberg, and M. Rogers, Plenum, New York, 1971, pp. 305–338.

[23]Epstein, R. J., and Bliss, D. B., "An Acoustic Boundary Element Method Using Analytical/Numerical Matching," *Journal of the Acoustical Society of America* (to be published).

[24]Epstein, R. J., and Bliss, D. B., "An Aeroacoustic Boundary Element Method Using Analytical/Numerical Matching," *Proceedings of the 1st Joint CEAS/AIAA Aeroacoustics Conference* (Munich, Germany), Vol. 1, Deutsche Gesellschaft fuer Luft- und Raumfahrt, Bonn, Germany, 1995, pp. 491–500.

[25]Jones, R. T., and Cohen, D., *Aerodynamics of Wings at High Speeds*, Vol. 7, Aerodynamics of Aircraft Components at High Speeds, Princeton Univ. Press, Princeton, NJ, 1957, Chap. 13.

[26]Van Dyke, M., *Perturbation Methods in Fluid Mechanics*, Parabolic, Stanford, CA, 1975, Chap. 4.

[27]Jones, R. T., *Wing Theory*, Princeton Univ. Press, Princeton, NJ, 1990, Chap. 8.

[28]Watkins, C., Woolston, D., and Cunningham, H. J., "A Systematic Kernel Function Procedure for Determining Aerodynamic Forces on Oscillating or Steady Finite Wings at Subsonic Speeds," NACA TR R-48, 1959, Chap. 8.

[29]Morino, L., "A General Theory of Unsteady Compressible Aerodynamics," NASA CR 2464, Dec. 1974.

[30]Ueda, T., and Dowell, E. H., "A New Solution Method for Lifting Surfaces in Subsonic Flow," *AIAA Journal*, Vol. 20, No. 3, 1982, pp. 348–355.

[31]Eversman, W., and Pitt, D. M., "Hybrid Doublet Lattice/Doublet Point Method for Lifting Surfaces in Subsonic Flow," *AIAA Journal*, Vol. 29, No. 9, 1991, pp. 572–578.